

Mid-infrared InAs/GaInSb separate confinement heterostructure laser diode structures

J. T. Olesberg, Michael E. Flatté,^{a)} and T. C. Hasenberg

Department of Physics and Astronomy and the Optical Science and Technology Center, University of Iowa, Iowa City, Iowa 52242

C. H. Grein

Department of Physics, University of Illinois at Chicago, Chicago, Illinois 60607

(Received 16 August 2000; accepted for publication 7 December 2000)

Despite recent progress in electronic structure engineering of type-II materials for mid-infrared lasers, suppression of Auger recombination at room temperature has been limited. We present an active region design, consisting of AlAsSb/InAs/GaInSb/InAs/AlAsSb wells separated by an InAs/AlGaSb superlattice, that overcomes this limitation. The 300 K calculated Auger recombination rate in this structure at the optimal lasing density is five times smaller than typical Shockley–Read–Hall (defect-assisted) recombination rates. An integrated separate confinement heterostructure design suitable for this active region is also described. The separate confinement region, which is a lightly doped InAs/AlGaSb superlattice, provides efficient hole transport and injection into the active region. For an estimated nonactive region modal cavity loss of 20 cm^{-1} and an optical mode width of $1.3 \text{ }\mu\text{m}$, the calculated internal threshold current density is 100 A/cm^2 at 300 K for a single quantum well device. © 2001 American Institute of Physics. [DOI: 10.1063/1.1346657]

I. INTRODUCTION

Mid-infrared materials based on the type-II InAs/GaInSb system are expected to have excellent optoelectronic properties for semiconductor laser applications.^{1–11} The large band offsets between InAs and GaInSb allow extensive tailoring of heterostructure materials to reduce the valence band density of states,^{2,3} eliminate intersubband absorption at the lasing wavelength,⁴ and suppress Auger recombination.^{1,2,7–9} Advances in these materials are expected to lead to laser diodes with high operating temperatures and output powers.^{5,6} However, both theoretical calculations and experimental results indicate that, in current materials, carrier lifetimes at room temperature lasing densities remain limited by Auger recombination.^{7–9}

The first InAs/GaInSb laser diodes used multiple quantum well active regions consisting of 3.5–6.5 periods of an InAs/GaInSb superlattice surrounded by GaInAsSb barriers.^{12,13} These devices lased from 2.8 to $4.3 \text{ }\mu\text{m}$ at temperatures as high as 255 K pulsed and 175 K continuous wave (for a $3.2 \text{ }\mu\text{m}$ device). However, edge effects in the thin InAs/GaInSb superlattice limited the optical and electronic properties of the active regions.⁴ Diodes based on a more highly optimized, strain-balanced InAs/GaInSb/InAs/AlGaInAsSb superlattice lased at $2.7 \text{ }\mu\text{m}$, but failed to lase at longer wavelengths under electrical injection. Diode structures with wavelengths of 4.0 and $5.3 \text{ }\mu\text{m}$ lased when optically pumped.¹⁴ Similar structures designed for optical pumping have lased above room temperature from 3.08 to $4.5 \text{ }\mu\text{m}$,^{15,16} and have lased at wavelengths as long as $7.3 \text{ }\mu\text{m}$ at temperatures of at least 220 K.¹⁷ Recently, diodes incor-

porating a separate confinement region have lased at $3.25 \text{ }\mu\text{m}$ at temperatures as high as 310 K pulsed and 180 K continuous wave.¹⁸

The large valence band offset between InAs and GaInSb, which is essential to the material optimization strategy, can significantly impede vertical hole transport. The failure of diodes based on thick active regions of the four-layer superlattice of Ref. 4 or the W structure of Ref. 3 to lase under electrical injection in noncascade diodes appears to be due to poor vertical hole transport in the superlattice active regions.¹⁹ Boltzmann relaxation-time approximation calculations for the four-layer superlattice of Refs. 7 and 8 indicate that the vertical hole mobility at 300 K is $2.6 \text{ cm}^2/\text{V s}$, assuming an empirical momentum relaxation time of 100 fs.²⁰ For a 3.0 ns carrier lifetime, this corresponds to a diffusion length of $\sim 0.14 \text{ }\mu\text{m}$, which is much shorter than the typical $0.4 \text{ }\mu\text{m}$ active region thickness. The resulting nonuniform carrier distribution in the active region would significantly degrade the performance of a laser diode. A superior design would improve vertical transport without compromising the optimization of other optical and electronic properties.

We describe here an integrated laser diode design that successfully addresses previous limitations due to Auger recombination and vertical hole transport. The calculated Auger lifetime of the active region material is longer than typical Shockley–Read–Hall (SRH) lifetimes, even at room temperature. In addition, the active region, separate confinement region, and cladding regions are specifically designed for efficient electrical injection and vertical transport. Calculations indicate that the room temperature internal threshold current density for a single-quantum-well laser diode could be as low as 100 A/cm^2 . Even if multiple wells are necessary due to large optical losses in the device, the threshold current

^{a)}Author to whom correspondence should be addressed; electronic mail: michael-flatte@uiowa.edu

density should be an order of magnitude smaller than previous type-II designs.

The electronic and optical properties of the material described here have been calculated using a 14-band superlattice $\mathbf{K}\cdot\mathbf{p}$ formalism.²¹ Earlier eight-band versions of this formalism have successfully predicted the density-dependent optical properties^{22,23} and Auger recombination rates^{7,8} of superlattices based on the InAs/GaInSb material system. The 14-band model naturally includes cubic anisotropy and the inversion asymmetry of zincblende semiconductors. It also reproduces the successes of the eight-band model in Refs. 7, 8, 22, and 23. We evaluate the Auger recombination rates using efficient Monte Carlo calculations of Fermi's golden rule employing this electronic structure and the derived momentum-dependent matrix elements.

The structure of this article is as follows: Section II summarizes the optimization process for mid-infrared type-II laser active regions. Section III focuses on the active region, whereas Sec. IV describes the details of the integrated diode design, including transport, injection, and optical confinement of the separate confinement region and clads.

II. OPTIMIZATION OF MID-INFRARED LASER ACTIVE REGIONS

A. Band-edge versus final-state optimizations

In order to design an optimal active region we consider several material properties, including differential gain, intersubband absorption, and Auger recombination. Electronic structure optimizations can be classified into two categories depending on the types of states affected.²⁴ The first category is band-edge optimization, which refers to strategies that alter the electronic structure near the valence and conduction band edges. This type of optimization has been well explored in near-infrared lasers, and generally involves reducing the density of states in the valence band in order to better balance the conduction and valence densities of states. Better balance in the densities of states produces lower threshold carrier densities and larger differential gains.^{25,26} Both Auger recombination and intersubband absorption increase with increasing carrier densities, so band-edge strategies to reduce the threshold carrier concentration reduce these processes indirectly. A noteworthy band-edge optimization strategy is the now endemic use of strain to reduce the valence band-edge degeneracy. Band-edge optimization strategies require moderate band offsets among material constituents.

The second category of optimizations is final state optimization, which refers to a practice of reducing the phase space for final states in the processes. Final state optimization has relevance for both intersubband absorption and Auger recombination. In intersubband absorption, which is a vertical process in momentum space, the relevant final states are one lasing energy away from the band edge occupied states for electrons and holes. Because type-II mid-infrared lasers lase in a transverse electric mode, intersubband absorption in the conduction band is minimal. Thus, final-state suppression of intersubband absorption requires control of states in the valence band approximately one band gap energy from the valence band edge. Much larger valence band

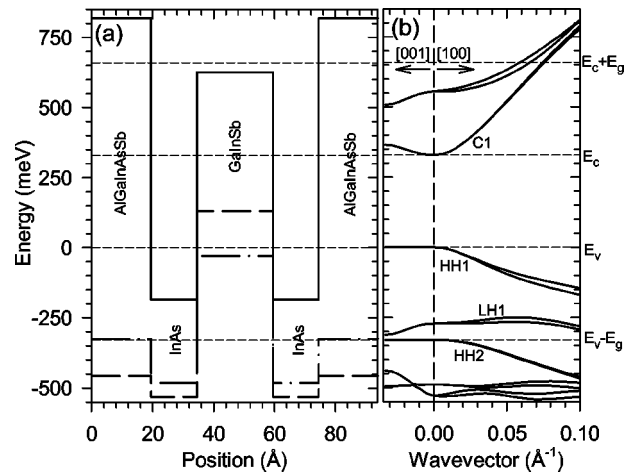


FIG. 1. (a) Bulk band edge energies and (b) superlattice band structure of the four-layer superlattice from Refs. 7 and 8. The solid line in (a) is the bulk conduction band energy, the dashed line is the bulk heavy-hole energy, and the dash-dot line is the bulk light-hole energy. The horizontal dashed lines indicate the superlattice conduction and valence band energies, along with the critical Auger and intersubband absorption energies. In (b), the band structure in the [001] (growth) direction is shown to the left of zero, the band structure in the [100] (in-plane) direction is shown to the right of zero.

offsets are required to achieve this than are required to achieve band-edge optimization; however, this goal has been accomplished at room temperature in previous type-II designs.^{3,4}

Figure 1 shows the band edges and band structure for a four-layer superlattice studied in Refs. 7 and 8. The band structure in Fig. 1(b) is shown along the [001] (growth) direction (with in-plane momentum equal to zero) and along the [100] (in-plane) direction (with growth direction momentum equal to zero). There is a gap in the electronic structure at the zone center roughly one energy gap from the top of the valence band. This gap, which extends throughout the growth-direction zone, is the origin of the final-state intersubband absorption optimization for this structure. However, because the Auger recombination is a nonvertical process, final states with large in-plane wave vector are also important.

The impact of intersubband absorption optimization can be quantified using the ratio of the net active region gain to the fundamental gain.^{5,6} This figure of merit is an intrinsic active region material quantity that measures the impact of intersubband absorption in the active region on the slope efficiency of a device. Optimized type-II designs can have active region material slope efficiencies (ratio of net material gain to total material gain) close to 100%.^{5,6}

B. Suppression of Auger recombination

Although balancing the densities of states at the band edge reduces Auger recombination, density of states balancing by itself is not sufficient to significantly suppress Auger recombination at room temperature. The use of final-state optimization to reduce Auger recombination involves eliminating final states for the carrier that absorbs the energy and momentum of the recombining electron-hole pair. Because the Auger process is not a vertical process, final state opti-

mization for Auger recombination is much more difficult to achieve than for intersubband absorption. Final-state optimization for Auger recombination has been shown to be effective at low temperature in the four-layer structures of Refs. 3, 4, and 7, but only minimally effective at room temperature.²⁴ To understand this we introduce details of the Auger recombination process in the four-layer superlattices.

The probability of an Auger event is proportional to the square of the screened Coulomb matrix element coupling the four states involved in the process. The screened Coulomb matrix element can be written as²⁷

$$|V_{\text{coulomb}}|^2 \propto \frac{\beta_{L_1, L_2}(\mathbf{K}_1, \mathbf{K}_2) \beta_{L_3, L_4}(\mathbf{K}_3, \mathbf{K}_4)}{[\lambda^2 + |\mathbf{K}_2 - \mathbf{K}_1|^2]^2} \times \delta(\mathbf{K}_2 - \mathbf{K}_1 - \mathbf{K}_4 + \mathbf{K}_3), \quad (1)$$

where λ is the reciprocal screening length. The scattering process involves the transition of an electron from superlattice state L_1 with wave vector \mathbf{K}_1 to state L_2 with wave vector \mathbf{K}_2 . The energy and momentum is transferred to an electron in state L_3 with wave vector \mathbf{K}_3 , which is promoted to state L_4 with wave vector \mathbf{K}_4 . For a typical hole–hole recombination process, L_1 will be the first conduction band, L_2 and L_4 are the top heavy-hole state, and L_3 will be a state deep in the valence band. The term $\beta_{L, L'}(\mathbf{K}, \mathbf{K}')$ describes the spatial overlap of superlattice states L and L' with wave vectors \mathbf{K} and \mathbf{K}' .

The momentum and energy structure of Auger processes can be understood from that of the Coulomb matrix element and the occupation factors of the four electronic states. We find that the matrix elements associated with the electron transition from the conduction band to the valence band are very similar for structures with and without final-state optimization. The role of final-state optimization can be seen most clearly by considering the transitions of the hole from the band-edge state (normally a HH1 state) to a state much lower in the valence band. The probability of such transitions from a HH1 state with in-plane momentum $\mathbf{K}_{\text{HH1}}^{\text{in-plane}}$ to a final state with in-plane momentum $\mathbf{K}_{\text{final}}^{\text{in-plane}}$ and energy E_{final} is proportional to

$$O(K_{\text{final}}^{\text{in-plane}}, E_{\text{final}}) = \frac{1}{K_{\text{max}}^z} \sum_L \int dK_L^z dK_{\text{HH1}}^z \times \beta_{L, \text{HH1}}(K_{\text{final}}^{\text{in-plane}}, K_L^z; K_{\text{HH1}}^{\text{in-plane}}, K_{\text{HH1}}^z) \times \delta[E_{\text{final}} - E_L(K_{\text{final}}^{\text{in-plane}}, K_L^z)], \quad (2)$$

where K_{max}^z is the width of the growth direction Brillouin zone. The integrations over the growth-direction zone account for the effect of growth-direction dispersion. Figure 2 shows $O(K_{\text{final}}^{\text{in-plane}}, E_{\text{final}})$ for the active region proposed in Ref. 4, and gives a visible indication of the strength of the coupling to near-zone-center HH1 states.

In order to identify the regions of greatest importance for Auger recombination, calculations of the Auger recombination rate were performed using a coarse grid for the 12-dimensional integration over momentum space. This resulted in a sampling of a few hundred of the most probable Auger transitions in the material for a given temperature and carrier

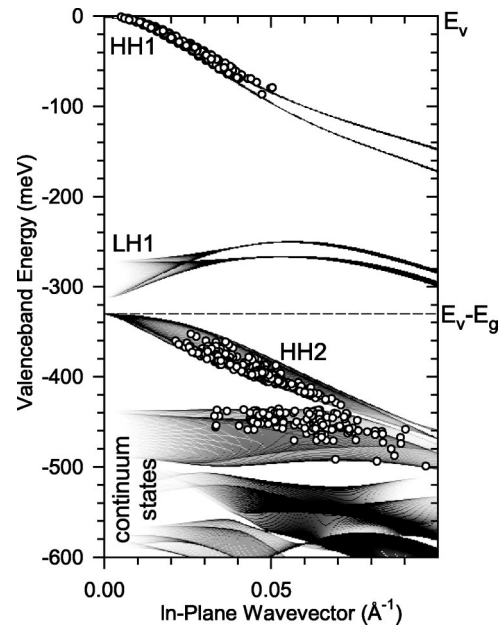


FIG. 2. Initial and final energies and in-plane wave vectors for the most probable hole–hole Auger transitions (open symbols) overlaid on the electronic structure of the valence band of a four-layer superlattice. The darkness of the gray scale is proportional to $O(K_{\text{final}}^{\text{in-plane}}, E_{\text{final}})$ from Eq. (2). In this half of the Auger process (the recombination of a conduction band electron with a hole is not shown), an electron is promoted from a state deep in the valence band to an unoccupied state (hole) near the top of the valence band.

density. The initial and final energies and wave vectors were recorded for the intervalence band portion of these transitions and are shown overlaid on the four-layer superlattice’s electronic structure in Fig. 2. Although a large gap is evident in the electronic structure at zone center, the relevant region for final states is near $K_{\text{final}}^{\text{in-plane}} \sim 0.05 \text{ \AA}^{-1}$, where the final-state gap is much smaller. Consequently, there is little final-state suppression in the four-layer superlattice at room temperature.

Because of the large gap in final states at the zone center, it was originally supposed that there would be large fluctuations in the Auger rate as states [such as LH1 or HH2 in Fig. 1(b) and Fig. 2] moved into and out of resonance with the band gap. However, only small changes (approximately a factor of 2) have been observed in experimental studies.⁹ This experimental result is in agreement with earlier detailed calculations of the Auger rate based on the electronic structure.²⁴ These results are now understood to be due to significant diminishing of the final-states gap away from the zone center.

Successful suppression of Auger recombination at room temperature requires a strategy for extending the final-states gap to finite in-plane wave vectors without compromising band-edge optimizations. Such a strategy has been developed and used in the design of an active region that is optimized for final-state Auger suppression at room temperature.

III. BROKEN-GAP QUANTUM WELL ACTIVE REGION

A broken-gap quantum well (BGQW) active region designed for emission at 3.4 \mu m is shown in Fig. 3.

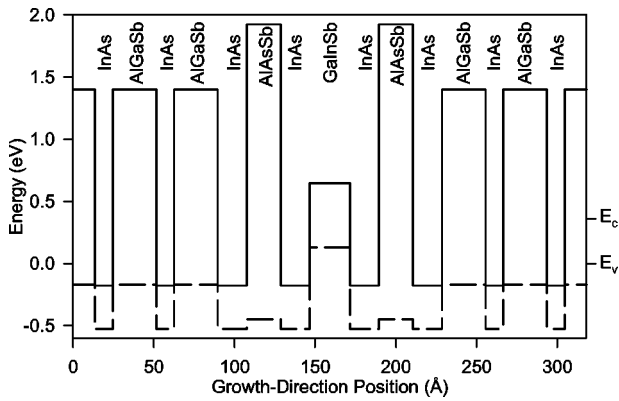


FIG. 3. Bulk band edge energies as a function of growth direction position for a 3.4 μm broken-gap quantum well. The solid line is the bulk conduction band energy and the dashed line is the bulk heavy-hole energy. The conduction and valence band energies of the superlattice are shown on the right of the figure.

The well consists of 21 Å AlAs_{0.15}Sb_{0.85}/15 Å InAs/25 Å Ga_{0.65}In_{0.35}Sb/15 Å InAs/21 Å AlAs_{0.15}Sb_{0.85}. The barrier surrounding the well is a 27 Å Al_{0.60}Ga_{0.40}Sb/11 Å InAs superlattice. The strain in the barrier superlattice and the quantum well is balanced so that the structure can be grown to arbitrary thicknesses on a GaSb substrate. Optimized designs over the 3–5 μm wavelength range are straightforward to generate with small changes in the well layer thicknesses. The band structure of this active region is shown in Fig. 4. Because of the large splitting between the top hole state and the rest of the valence band states, the valence band density of states is relatively small (~ 1.6 times that of the conduction band).

It is not immediately apparent from Fig. 4 that this material also demonstrates final-state optimization. In contrast with Fig. 1(b), there are valence band states in the relevant energy range for intersubband and Auger recombination transitions. If one examines the intersubband absorption, however (shown in Fig. 5), there is a clear suppression of

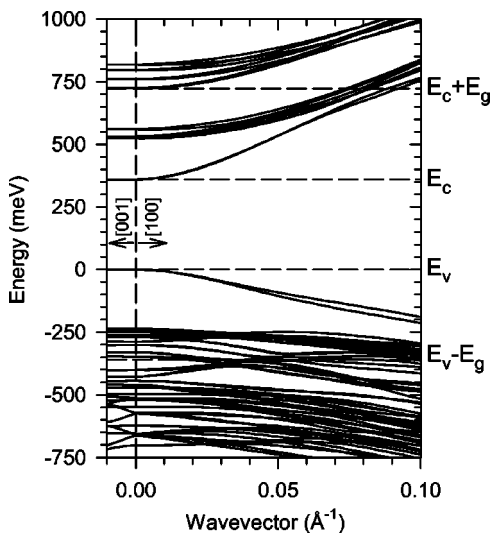


FIG. 4. Band structure of the 3.4 μm broken-gap quantum well. The band structure in the [001] (growth) direction is shown to the left of zero; the band structure in the [100] (in-plane) direction is shown to the right of zero.

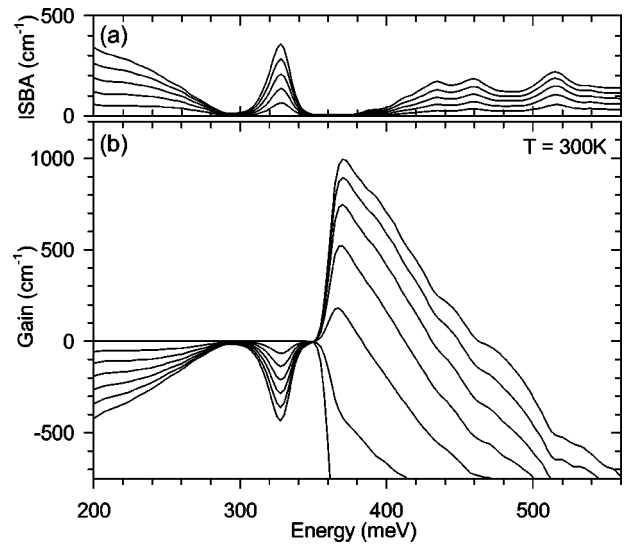


FIG. 5. (a) Intersubband absorption and (b) gain spectra for the 3.4 μm BGQW. Curves are shown for carrier densities of 1, 2, 3, 4, and 5 $\times 10^{17} \text{ cm}^{-3}$. There is significant suppression of intersubband absorption at photon energies near the peak of the gain spectrum, which results in a large slope-efficiency figure of merit for this active region.

intersubband absorption processes near the peak of the gain spectrum. The states that appear to be plausible final states for intervalence band absorption in Fig. 4 (those with energies around -350 meV) are in fact localized in the barriers, while the initial state for intersubband absorption (HH1) is localized in the GaInSb well. Because of this, the matrix elements for transitions from the top of the valence band to these states are negligible. This can be seen by examining the envelope functions for these states. Figure 6 shows the norm of the zone-center envelope functions as a function of energy and growth-direction position. The first conduction band state (C1) is localized across the central InAs/GaInSb/InAs layers while the first valence band state (HH1) is strongly localized in the GaInSb layer. Below the third valence band well state (HH2), there is a 150 meV gap in the zone-center electronic structure in the central well layers, even though

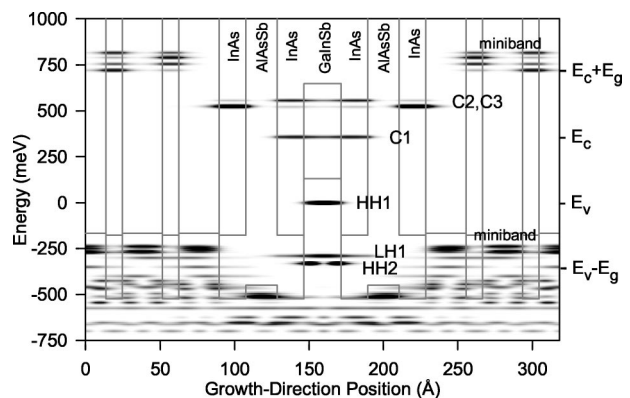


FIG. 6. Spatial distribution of the zone-center superlattice states. The darkness of each point is proportional to the norm of the envelope function at that position. There is a spatial gap in the valence band structure in the central layer (below HH2) that is responsible for final-state optimization. The LH1 state in the middle is resonant with the band edge states of the superlattice, enhancing vertical transport (see Ref. 19).

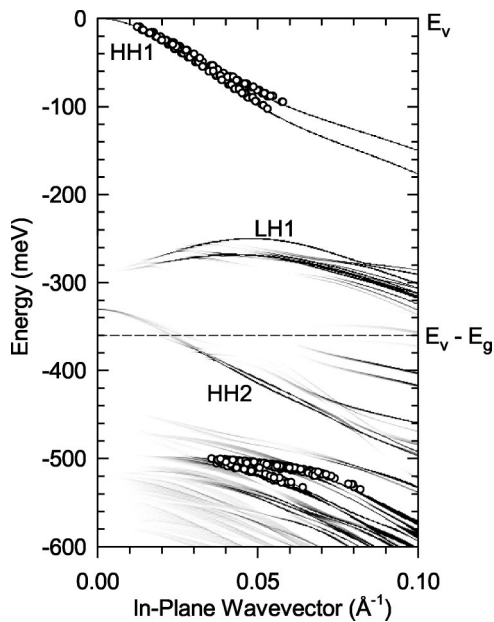


FIG. 7. Initial and final energies and in-plane wave vectors for the most probable hole Auger transitions (open symbols) overlaid on the electronic structure for the 3.4 μm BGQW. The scale of the coupling strength is the same as in Fig. 2.

there are barrier states at those energies. This “spatial gap” in the electronic structure in the energy range located one lasing mode photon energy below the top heavy hole state in the well is the origin of final-state intersubband absorption optimization in this material. The resulting slope efficiency figure of merit for this material is 99%.

The spatial gap in the valence band structure is a consequence of the InAs/AlAsSb/InAs layers surrounding the GaInSb well. These potential barriers isolate the GaInSb well states from those of the superlattice barrier down to energies around -500 meV. The exception to this is the first light-hole state (LH1), which is localized primarily in the GaInSb layer but extends significantly into the barrier superlattice. LH1 is an extended state that facilitates capture from the superlattice barrier into the GaInSb well, as proposed in Ref. 19. The presence of a distributed state in the midst of a spatial gap is analogous to the conduction band structure of a resonant tunneling diode.

Whereas the electronic structure features seen in Fig. 6 are zone-center features, the spatial gap exists in the electronic structure at finite in-plane momentum as well. Figure 7 shows the electronic structure of the BGQW shown in a similar fashion to Fig. 2 for the four-layer superlattice. The key for reducing Auger recombination at room temperature is extending the gap in the final states for Auger processes farther out in the in-plane direction. The final-states gap in the electronic structure at in-plane wave vectors of ~ 0.05 \AA^{-1} is approximately 60 meV, which is more than twice as large as in the four-layer superlattice. In addition, the states on the lower edge of the gap (around -480 meV) are only weakly coupled to the top of the valence band due to the spatial isolation of the states from each other. We also note that the size of the final-states gap, which is greater than the energy of an optical phonon, suggests that phonon-assisted

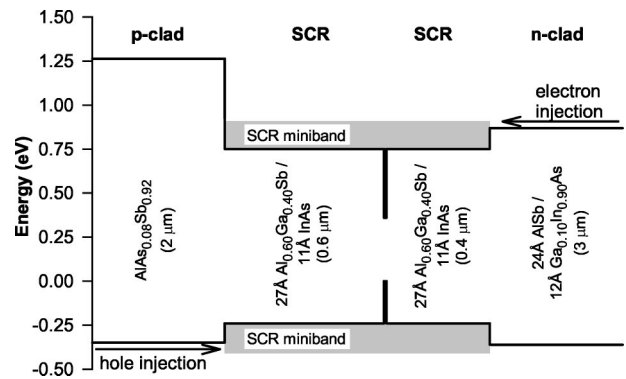


FIG. 8. Schematic of the laser diode structure that includes a single quantum well active region, lightly doped separate confinement regions, and heavily doped clads. The estimated mode width and nonactive-region modal losses for this structure are 1.3 μm and 20 cm^{-1} , respectively.

Auger recombination will be suppressed as well. The most probable Auger transitions for this material involve valence band continuum states 500 meV from the valence band edge. The net result is that the calculated Auger recombination rate is reduced by almost 2 orders of magnitude with respect to the four-layer superlattice at the optimal densities for lasing.

The calculated room temperature Auger recombination rate at the optimal density for lasing is 0.06 ns^{-1} . The calculated radiative rate at this density is also 0.06 ns^{-1} . Because these rates are much smaller than the typical 0.3 ns^{-1} rate due to SRH processes, the system is expected to be SRH limited at room temperature. The total carrier lifetime at the optimum density for lasing is 2.5 ns, which is six times longer than for the four-layer superlattice of Refs. 7 and 8.

The dependence of the optimum lasing threshold of a device on the active region depends principally on a cavity-independent figure of merit: the optimal ratio of the net active region gain to the volumetric recombination current density.^{5,6} Assuming a 3.0 ns SRH lifetime, the figure of merit for the BGQW is 2900 $\mu\text{m}^2/\text{A}$ at 300 K.²⁸ This value far exceeds that of other mid-infrared materials (~ 40 – 75 for type-I quantum wells and ~ 260 for type-II superlattices).^{5,6} Because the threshold current density is inversely proportional to this figure of merit, lasing thresholds for this structure should be more than an order of magnitude smaller than current interband diodes. The large net material gain (625 cm^{-1}) at the optimal density suggests that a single quantum well active region should be sufficient for lasing in a suitably designed cavity. We now describe such a cavity.

IV. INTEGRATED DIODE DESIGN

An optimized cavity designed for this active region is shown in Fig. 8. An essential feature of this cavity is a separate confinement region (SCR) that reduces the mode overlap with the highly doped clads and has good vertical hole mobility. The SCR of the cavity is 0.4 μm thick on the *n* side and 0.6 μm thick on the *p* side. Recent work in near-infrared diode development (2.0–2.7 μm) has demonstrated the importance of such SCRs for high-temperature and high-power operation.^{29–31} The material used for the SCR is the same InAs/AlGaSb superlattice that is used as the quantum-well

TABLE I. Calculated internal threshold current density (A/cm^2) as a function of nonactive-region optical loss and number of quantum wells. For each cavity, the minimum current density is boldface.

Wells	$\alpha_m + \langle \alpha_w \rangle$		
	20 cm^{-1}	50 cm^{-1}	100 cm^{-1}
1	102	-	-
2	97	404	-
3	119	228	-
4	145	227	808
5	171	242	510
7	224	286	447
10	303	362	485

barrier in the active region. It is lattice matched to the GaSb substrate and has a larger index of refraction ($n \sim 3.45$) than the doped clads.

The vertical mobility of holes in this superlattice has been calculated using the linear Boltzmann equation, assuming an energy independent momentum scattering time, but without additional approximations to the calculated electronic structure. Scattering due to interface fluctuations in layer thicknesses is expected to dominate the momentum scattering time, and that scattering is energy-independent. In the four-layer superlattice a 100 fs momentum scattering time reproduced the measured in-plane ambipolar diffusion of optically excited carriers.²⁰ Assuming that the momentum scattering time for electrons and holes is the same we find a vertical hole mobility of $160\text{ cm}^2/V\text{ s}$ for a doping level of $1 \times 10^{17}\text{ cm}^{-3}$. This vertical hole mobility, which is comparable with that of bulk InAs and is 2 orders of magnitude larger than that of the four-layer superlattice, ensures good vertical transport between the clads and the active region. Because the SCR is a superlattice, it is straightforward to grade its band edges by varying the superlattice period. This can be used to match the band edges of the SCR to the injection level of the clads or to localize injected carriers near the active region.

The $\text{AlAs}_{0.08}\text{Sb}_{0.92}$ p clad has a small index of refraction ($n \sim 3.23$), a large confining potential for electrons, and a well-matched hole injection level with the superlattice clad. The $24\text{ \AA AlSb}/12\text{ \AA Ga}_{0.10}\text{In}_{0.90}\text{As}$ superlattice n clad ($n \sim 3.33$) provides electron injection matched to the miniband of the separate confinement superlattice and allows n doping with silicon.

Based on optical mode calculations for a 2 mm long cavity with uncoated facets, we estimate the sum of the mirror losses (α_m) and nonactive-region modal waveguide losses ($\langle \alpha_w \rangle$) for the cavity described above to be $\alpha_m + \langle \alpha_w \rangle = 20\text{ cm}^{-1}$. The optical confinement factor is 2.1% for a single quantum well in this cavity. Because active region losses due to intersubband absorption are included in the calculation of the *net* active region gain, they are not included in the cavity loss value. The calculated internal threshold current density for a single quantum well device is 100 A/cm^2 .³² The use of a few quantum wells significantly reduces the problem of nonuniform carrier distribution in the active region.

In order to evaluate the impact of varying optical losses, we show in Table I calculated internal threshold current densities for the BGQW active region at 300 K for a series of cavity losses and numbers of wells. Even for the largest loss case (100 cm^{-1}), lasing is achievable with four wells at 810 A/cm^2 . Recently, total modal losses of 50 and 100 cm^{-1} have been observed in structures without separate confinement regions (these *total* loss values include intersubband absorption losses in the active region).^{16,33}

V. CONCLUDING REMARKS

When direct Auger recombination processes are reduced substantially, other processes, such as phonon-assisted and elastic scattering assisted Auger recombination (from, e.g., interface roughness) may dominate. We have not calculated these rates, but note that the size of the gap in the electronic structure near the region of Auger final states is much larger than the energy of an optical phonon. Thus, close-to-vertical phonon-assisted Auger should be suppressed. A greater uncertainty is the significance of scattering assisted Auger recombination involving large momentum transfers. In these phonon or impurity-assisted scattering processes, a large in-plane momentum is transferred to the carrier, which allows it to make a transition to states far from the zone center.

We note that studies of thermal conductivity of superlattices suggest that superlattice separate confinement regions may have low thermal conductivity. The diode lasing results of Ref. 14, however, were obtained with superlattice clads similar to those presented here. Future studies will explore this topic.

The BGQW active region is calculated to have a factor of 6 increase in the carrier lifetimes at room temperature lasing densities with respect to a comparable four-layer superlattice and is designed specifically for electrical injection. The threshold figure of merit for the active region is $2900\text{ }\mu\text{m}^2/\text{A}$ at room temperature, while the slope efficiency figure of merit is 99%. The integrated separate confinement region superlattice has a hole vertical mobility of the same order as bulk InAs and well-matched band edges for transport. For a low-loss cavity, the internal threshold current density of a laser diode is expected to be as low as 100 A/cm^2 at room temperature for a single quantum well diode emitting at $3.4\text{ }\mu\text{m}$.

ACKNOWLEDGMENTS

This research was supported in part by the U.S. Air Force, Air Force Materiel Command, Air Force Research Laboratory, Kirtland AFB, New Mexico, 87117-5777 (Contract No. F29601-97-C-0041) and the National Science Foundation (Grant Nos. ECS-97007799, ECS-9900486, and ECS-0000556).

¹C. H. Grein, P. M. Young, and H. Ehrenreich, J. Appl. Phys. **76**, 1940 (1994).

²M. E. Flatté, C. H. Grein, H. Ehrenreich, R. H. Miles, and H. Cruz, J. Appl. Phys. **78**, 4552 (1995).

³J. R. Meyer, C. A. Hoffman, F. J. Bartoli, and L. R. Ram-Mohan, Appl. Phys. Lett. **67**, 757 (1995).

⁴M. E. Flatté, J. T. Olesberg, S. A. Anson, T. F. Boggess, T. C. Hasenberg, R. H. Miles, and C. H. Grein, Appl. Phys. Lett. **70**, 3212 (1997).

⁵J. T. Olesberg, M. E. Flatté, B. J. Brown, C. H. Grein, T. C. Hasenberg, S.

- A. Anson, and T. F. Boggess, *Appl. Phys. Lett.* **74**, 188 (1999).
- ⁶J. T. Olesberg, M. E. Flatté, B. J. Brown, T. C. Hasenberg, S. A. Anson, T. F. Boggess, and C. H. Grein, *Proc. SPIE* **3628**, 148 (1999).
- ⁷D.-J. Jang, M. E. Flatté, C. H. Grein, J. T. Olesberg, T. C. Hasenberg, and T. F. Boggess, *Phys. Rev. B* **58**, 13047 (1998).
- ⁸M. E. Flatté, C. H. Grein, T. C. Hasenberg, S. A. Anson, D.-J. Jang, J. T. Olesberg, and T. F. Boggess, *Phys. Rev. B* **59**, 5745 (1999).
- ⁹J. R. Meyer *et al.*, *Appl. Phys. Lett.* **73**, 2857 (1998).
- ¹⁰I. Vurgaftman, J. R. Meyer, and L. R. Ram-Mohan, *IEEE Photonics Technol. Lett.* **9**, 170 (1997).
- ¹¹I. Vurgaftman, J. R. Meyer, F. H. Julien, and L. R. Ram-Mohan, *Appl. Phys. Lett.* **73**, 711 (1998).
- ¹²D. H. Chow, R. H. Miles, T. C. Hasenberg, A. R. Kost, Y.-H. Zhang, H. L. Dunlap, and L. West, *Appl. Phys. Lett.* **67**, 3700 (1995).
- ¹³T. C. Hasenberg, R. H. Miles, A. R. Kost, and L. West, *IEEE J. Quantum Electron.* **33**, 1403 (1997).
- ¹⁴M. E. Flatté, T. C. Hasenberg, J. T. Olesberg, S. A. Anson, T. F. Boggess, C. Yan, and D. L. McDaniel, Jr., *Appl. Phys. Lett.* **71**, 3764 (1997).
- ¹⁵C. L. Felix, J. R. Meyer, I. Vurgaftman, C.-H. Lin, S. J. Murry, D. Zhang, and S.-S. Pei, *IEEE Photonics Technol. Lett.* **9**, 734 (1997).
- ¹⁶W. W. Bewley *et al.*, *Appl. Phys. Lett.* **73**, 3833 (1998).
- ¹⁷D. W. Stokes, L. J. Olafsen, W. W. Bewley, I. Vurgaftman, C. L. Felix, E. H. Aifer, J. R. Meyer, and M. J. Yang, *J. Appl. Phys.* **86**, 4729 (1999).
- ¹⁸W. W. Bewley *et al.*, *Appl. Phys. Lett.* **76**, 256 (2000).
- ¹⁹M. E. Flatté, J. T. Olesberg, and C. H. Grein, *Mater. Res. Soc. Symp. Proc.* **484**, 71 (1998).
- ²⁰S. A. Anson, J. T. Olesberg, M. E. Flatté, T. C. Hasenberg, and T. F. Boggess (unpublished).
- ²¹J. T. Olesberg, Ph.D. thesis, The University of Iowa, 1999.
- ²²J. T. Olesberg, S. A. Anson, S. W. McCahon, M. E. Flatté, D. H. Chow, and T. C. Hasenberg, *Appl. Phys. Lett.* **72**, 229 (1998).
- ²³S. A. Anson, J. T. Olesberg, M. E. Flatté, T. C. Hasenberg, and T. F. Boggess, *J. Appl. Phys.* **86**, 713 (1999).
- ²⁴M. E. Flatté and C. H. Grein, *Opt. Express* **2**, 131 (1998).
- ²⁵A. R. Adams, *Electron. Lett.* **22**, 249 (1986).
- ²⁶E. Yablonovitch and E. O. Kane, *J. Lightwave Technol.* **4**, 504 (1986).
- ²⁷C. H. Grein, P. M. Young, M. E. Flatté, and H. Ehrenreich, *J. Appl. Phys.* **78**, 7143 (1995).
- ²⁸In the limit that SRH recombination becomes negligible, the figure of merit due to intrinsic processes (Auger and radiative recombination) is $12\,000\ \mu\text{m}^2/\text{A}$.
- ²⁹D. Z. Garbuzov, R. U. Martinelli, H. Lee, P. K. York, R. J. Menna, J. C. Connolly, and S. Y. Narayan, *Appl. Phys. Lett.* **69**, 2006 (1996).
- ³⁰D. Z. Garbuzov *et al.*, *Appl. Phys. Lett.* **70**, 2931 (1997).
- ³¹D. Z. Garbuzov, H. Lee, V. Khalfin, R. Martinelli, J. C. Connolly, and G. L. Belenky, *IEEE Photonics Technol. Lett.* **11**, 794 (1999).
- ³²In the limit that SRH recombination is negligible, this value becomes $72\ \text{A}/\text{cm}^2$.
- ³³H. Q. Le, C. H. Lin, S. J. Murray, R. Q. Yang, and S. S. Pei, *IEEE J. Quantum Electron.* **34**, 1016 (1998).